Dynamics of Dry Friction: A Numerical Investigation

Y. F. Lim and Kan Chen
Department of Computational Science, National University of Singapore, Singapore 119260
(February 1, 2008)

We perform extended numerical simulation of the dynamics of dry friction, based on a model derived from the phenomenological description proposed by T. Baumberger et al. [1,2]. In the case of small deviation from the steady sliding motion, the model is shown to be equivalent to the state- and rate-dependent friction law which was first introduced by Rice and Ruina [3] on the basis of experiments on rocks. We obtain the dynamical phase diagram that agrees well with the experimental results on the paper-on-paper systems. In particular, the bifurcation between stick-slip and steady sliding are shown to change from a direct (supercritical) Hopf type to an inverted (subcritical) one as the driving velocity increases, in agreement with the experiments.

PACS numbers: 05.45.+b, 46.30.Pa, 62.20.Hg, 91.30.Px

I. INTRODUCTION

It is well-known that the frictional resistance is independent of the apparent area of the sliding surface and it is proportional to the normal load with a proportional constant μ, which is known as the friction coefficient. Traditionally, the friction coefficient has two distinct values: the static friction coefficient μ_s, determined from the minimum force needed to move a slider at rest, and the dynamic friction coefficient μ_d, used for the friction force when a steady sliding motion is established. Friction is often described using the well-known Amontons-Coulomb's laws: (i) both μ_s and μ_d are independent of the apparent area of the contacting surfaces and the normal load; (ii) both μ_s and μ_d depend on the shear characteristics of the contacting materials [4,5]; (iii) for most cases, μ_d is appreciably lower than μ_s. This standard picture is still widely accepted nowadays; however, in many cases, significant refinements must be taken into account for the explanation of the observed friction.

Our common experiences tell us that the sliding of contact bodies subjected to a steady pulling velocity sometimes proceeds in an alternation of periods of rest and slide rather than moving steadily (this is the reason, for example, for the occurrence of squeaking noises). This unstable motion consists of periods of a stick state followed by a sudden slip is known as stick-slip oscillations. The stick-slip motion occurs on both large and small scales. Understanding stick-slip phenomenon is not only important for many engineering applications, but also for understanding the mechanism of earthquakes (which is a stick-slip phenomenon at geological scale [6]).

Obviously, stick-slip is caused by the variation of frictional resistance during sliding. In certain range of the velocity V, a velocity weakening behavior (corresponding to a decreasing function $\mu_d(V)$ with respect to the steady relative sliding velocity V of the contact surfaces) is often observed in many different materials including metals [5] and rocks [7]. In this range, which generally lies in low-velocity regime, the steady motion is unstable with respect to perturbation; this gives rise to stick-slip phenomena. On the other hand, the static friction coefficient μ_s is generally found to be an increasing function with respect to the contact age of contact surfaces [7,8]. This can be explained by the fact that the plastic relaxation of the stressed contact junctions during a stick period leads to an increasing real contact area, hence strengthening the contact. The mechanism for the velocity-dependence of μ_d and the mechanism for the age-dependence of μ_s are not un-related; both can be understood using the concept of a memory length [7].

The purpose of the paper is to show, by explicit numerical simulation, that the model based on the phenomenological description of Ref. [2] can be used to explain qualitatively (and sometimes even quantitatively) many interesting features found in experiments. The model incorporates the existing understanding of the age-dependence of the static friction and the velocity-dependence of the dynamic friction at low velocity, but does not make a distinction between the dynamic and static frictions. There is no abrupt change from "static" friction to "dynamic" friction as in the traditional description of friction; this is important for numerical simulation used to construct the entire phase diagram for the dynamics of dry friction. The rest of the paper is organized as follows. We first review the phenomenology of dry friction, focusing on the recent experiments by T. Baumberger et al. [1,2]. We then show that the phenomenological description of Ref. [2] is equivalent to the well-known Rice-Ruina friction law on rock friction in the case of small deviation from the constant velocity motion [3]. The results from simulation of the model will be presented in the last section together with some concluding remarks.

II. PHENOMENOLOGY OF DRY FRICTION

Following the pioneering work of Rabinowicz on metals [5], many experimental studies have been performed to study the low velocity friction properties of various materials. It is beyond the scope of the paper to review these experimental work on the dynamics of dry friction. Instead, we focus on a recent extensive experimental study of the dry friction dynamics of a paper-on-paper block-spring system (shown in Fig. 1) by T. Baumberger et al. [1,2]. Their experiments verified many known properties of dry friction and gave a rather complete picture of dry friction in various regimes. In particular, they explored systematically the dynamical phase diagram by varying the driving velocity V, the slider mass M and the spring stiffness K. The features of their experiments are summarized as follows.

- The phase diagram in control parameter space $(V, K/M)$ consists of two regions that can be characterized by stick-slip and steady sliding respectively and they are separated by a bifurcation curve. The character of the bifurcation changes from a direct (supercritical) Hopf type in the creep-dominated regime to an inverted (subcritical) one in the inertial regime as V increases.

- In the steady sliding region, the measured dynamic friction coefficient μ_d exhibits velocity weakening in low-velocity range ($\leq 0.1mm/s$) which can be fitted as

$$\mu_d(V) \mid_{lowV} = a_v - b_v \ln(V/V_0), \tag{1}$$

  where V_0 is an arbitrary velocity scale; and velocity strengthening at larger velocities which can be characterized as

$$\mu_d(V) \mid_{highV} = \mu_d^0 + \eta V. \tag{2}$$

- The static friction coefficient μ_s was found to increase with the contact age t_{st} as

$$\mu_s(t_{st}) = a_s + b_s \ln(t_{st}). \tag{3}$$

- By introducing a characteristic memory length D_0, a relation between Eq. 1 and Eq. 3, i.e.

$$\mu_d(V) \mid_{lowV} = \mu_s(D_0/V) \tag{4}$$

  can be established. Here D_0, which is given experimentally as $0.9\mu m$ [2], can be interpreted as an average sliding displacement needed to move to new micro-contacts.

These results are rather general (rock-rock friction, for example, exhibits similar features). The experiments show that the motion of the system at low-velocity ($\leq 0.1mm/s$) is primarily controlled by a creep process. Based on these results, a phenomenological model of dry friction dynamics at low-velocity regime [2] of the paper-on-paper system has been proposed. Both linear [2] and nonlinear [9] stability analysis of the model near the bifurcation give excellent quantitative agreements with experiments. Beside this, the transient behavior in the steady sliding region of the system after setting the driving velocity to zero suddenly has been studied under the aid of the model [10], where two-stage process has been observed. However, there is no systematic theoretical study of the entire regime covering the crossover from the "static" friction regime to the "dynamic" friction regime and the crossover to the high-velocity (inertial) regime. In this paper we show numerically that most important experimental features in various regimes can be reproduced in a single model.

III. A PHENOMENOLOGICAL MODEL

We follow the phenomenological approach used in Ref. [2]. Consider the experimental setup shown in Fig. 1. The motion of the block under the influence of the external driving force as shown in Fig. 1, is assumed to be a thermally activated creeping motion in a periodic pinning potential biased by the external driving force. In the low bias regime, where the barrier heights of the effective potential are comparable with the thermal activation energy, the velocity of the slider is given by

$$\dot{x} = a(\frac{1}{\tau_+} - \frac{1}{\tau_-}), \tag{5}$$

where a is the typical distance between two potential minima, and τ_+ (τ_-) is the thermal time for escaping from a given well into its downstream (upstream) nearest neighbor. If we let the corresponding barrier height to be U_+ (U_-), then we have

$$\frac{1}{\tau_\pm} = \frac{\omega_0}{2\pi} \exp\{-\frac{\Delta U_\pm}{\sigma}\}, \tag{6}$$

where σ is the thermal activation energy. σ can be written as $N_{cr}RT$, where N_{cr} is the number moles of the degrees of freedom involved in the creep motion. ω_0 is the oscillation frequency about the minimum of the effective potential. The amplitude ΔU_0 of the periodic pinning potential is assumed to increase with the dynamical contact age variable ϕ defined in Ref. [2], hence the barrier heights are given by

$$\Delta U_\pm = \Delta U_0(\phi) \mp F_{ext}a/2, \tag{7}$$

where F_{ext} is the external force (in the experimental setup, it is the spring force induced by the driving velocity V).

Although Eqs. 5 and 6 are valid strictly only for a time- and position-independent external force and a time-independent pinning potential, they can also be used in more general cases under the assumption that the changes in F_{ext} and $\Delta U_0(\phi)$ are so slow that an *adiabatic* approximation is valid. Combining the above equations we can write the velocity of the slider as

$$\dot{x}(t) \approx \frac{\omega_0 a}{2\pi} 2\sinh\{\frac{F_{ext}a}{2\sigma}\} \exp\{-\frac{\Delta U_0}{\sigma}\}. \tag{8}$$

In the case that $F_{ext}a \gg \sigma$, the above equation can be approximated as

$$F_{ext} = \frac{2\Delta U_0(\phi)}{a} + \frac{2\sigma}{a} \ln(\frac{2\pi\dot{x}}{\omega_0 a}). \tag{9}$$

We now proceed to derive $U_0(\phi)$ by considering the case of constant velocity motion ($\dot{x} = V$). In this case $\phi = D_0/V$, and the friction force (given in Eq. 1) is equal to the external force F_{ext} given in Eq. 9. This gives rise to

$$Mg(a_v - b_v \ln(V/V_0)) = \frac{2\Delta U_0(\phi)}{a} + \frac{2\sigma}{a} \ln(\frac{2\pi V}{\omega_0 a}).$$

By using the average contact age ϕ, we can rewrite the above equation as

$$\Delta U_0(\phi) = \frac{a}{2} Mg\{a_v - b_v \ln\frac{D_0}{V_0} - A\ln\frac{2\pi D_0}{\omega_0 a} + (b_v + A)\ln\phi\}, \tag{10}$$

where $A = 2\sigma/aMg$. Given $U_0(\phi)$, we can write the friction coefficient (which is equal to the external force divided by the weight Mg under the quasi-stationary approximation) in term of ϕ

$$\mu(\phi, \dot{x}) = a_v + b_v \ln\frac{\phi V_0}{D_0} + A\ln\frac{\phi\dot{x}}{D_0}. \tag{11}$$

When the velocity is not a constant, the contact age ϕ is assumed to satisfy the following equation

$$\dot{\phi}(t) = 1 - \frac{\dot{x}\phi}{D_0}. \tag{12}$$

By using this equation, the rate-dependence of the dynamic friction and the contact time dependence of the static friction can be taken into account properly. Eqs.11 and 12 form the basis for the phenomenological description of dry friction given in Ref. [2].

We now show that this description of friction is in fact equivalent to the state- and rate-dependent friction law proposed by Rice and Ruina [3] in the case of small deviation from constant velocity motion. To make this connection, we choose $\theta = \ln(\phi V_0/D_0)$ (θ is the state variable in the Rice-Ruina theory), then Eqs.11 and 12 become

$$\mu(\theta, \dot{x}) = a_v + A\ln\frac{\dot{x}}{V_0} + (b_v + A)\theta, \tag{13}$$

$$\dot{\theta}(t) = \exp\{-\theta + \ln\frac{V_0}{D_0}\} - \frac{\dot{x}}{D_0}. \tag{14}$$

In Rice-Ruina theory, the dynamical equations for the friction coefficient μ and state variable θ in the state- and rate-dependent friction law [3] can be expressed as [11]

$$\mu(\theta, \dot{x}) = \mu_0 + A' \ln \frac{\dot{x}}{V_0} + B'\theta, \tag{15}$$

$$\dot{\theta}(t) = -\frac{\dot{x}}{D_0}\{\theta + \ln \frac{\dot{x}}{V_0}\}. \tag{16}$$

Consider the case that there is only a small deviation from the steady sliding state, we write

$$\dot{x}(t) = V + \Delta\dot{x},$$
$$\theta(t) = -\ln \frac{V}{V_0} + \Delta\theta.$$

Expending Eqs. 14 and 16 to first order of $\Delta\dot{x}$ and $\Delta\theta$ give the same dynamical equation for $\Delta\theta$,

$$\frac{d(\Delta\theta)}{dt} = -\frac{V\Delta\theta}{D_0} - \frac{\Delta\dot{x}}{D_0}. \tag{17}$$

By choosing $a_v = \mu_0$, $A = A'$ and $b_v + A = B'$, Eqs. 13 and 15 are exactly the same. Thus these two descriptions are in fact equivalent in the case where the deviation from the steady sliding motion is small. This is a strong indication that the phenomenological theory of dry friction discussed in Ref. [2] is not limited to the explanation of experimental results on the paper-on-paper system, but a rather general theory that can be used as a basis for studying the dynamics involving dry friction on a range of materials. For example, it will be useful for studying rock friction, which is important in the study of earthquake dynamics.

For the case where σ is comparable with $F_{ext}a$ (this can be thought of as in the *static friction* regime), we have to use the original equation, i.e. Eq. 8, which can be rewritten as

$$F_{ext}(\phi, \dot{x}) = MgA \sinh^{-1}\{\frac{\pi\dot{x}}{\omega_0 a} \exp[\frac{\Delta U_0(\phi)}{\sigma}]\}. \tag{18}$$

The friction coefficient is then given as (with quasi-stationary approximation)

$$\mu(\phi, \dot{x}) = Asign(\dot{x}) \sinh^{-1}\{\frac{1}{2} \exp[\frac{\bar{\mu}}{A}]\}, \tag{19}$$

where

$$\bar{\mu} = a_v + b_v \ln \frac{\phi V_0}{D_0} + A \ln \frac{\phi|\dot{x}|}{D_0}; \tag{20}$$

here, $\bar{\mu}$ is an approximation of μ we describe in Eq. 11. In this *static friction* regime, the velocity $\dot{x}$ is very small and it can also change its sign, thus the equation for ϕ needs to be modified. It is reasonable to simply use

$$\dot{\phi}(t) = 1 - \frac{|\dot{x}|\phi}{D_0}. \tag{21}$$

There are a few advantages of using Eqs.19, 20, and 21 to describe friction force: (*i*) there is no need to make a distinction between *static* and *dynamic* frictions, thus there is no *stopping* condition (which is used to indicate the crossover from the "dynamic" friction regime to the "static" friction regime) to worry about; (*ii*) the contact age is a well-defined quantity with Eq. 21; (*iii*) There is no numerical singularity in the dynamical equations for the sliding block when the velocity goes to zero and changes sign.

To include the inertial regime, we have to take into account the velocity strengthening described by Eq. 2; we include this effect by simply adding a damping term $\eta\dot{x}$ in Eq. 19.

IV. PHASE DIAGRAM OF DRY FRICTION DYNAMICS

We now present the numerical results from the simulation of the block-spring system. Using the friction law described in the previous section, we can write down the dynamical equations of the block-spring system shown in Fig. 1.

$$M\ddot{x}(t) = K(Vt - x) - \mu(\phi, \dot{x})N, \tag{22}$$

where

$$\mu(\phi, \dot{x}) = A sign(\dot{x}) \sinh^{-1}\{\frac{1}{2}\exp[\frac{\bar{\mu}}{A}]\} + \eta\dot{x}, \tag{23}$$

$$\bar{\mu} = a_v + b_v \ln\frac{\phi V_0}{D_0} + A\ln\frac{\phi|\dot{x}|}{D_0}, \tag{24}$$

and

$$\dot{\phi}(t) = 1 - \frac{|\dot{x}|\phi}{D_0}. \tag{25}$$

We compare our result for the friction coefficient $\mu = \mu(D_0/V, V)$ with the experimental results when the sliding motion is steady ($\dot{x} = V$ and $\phi = D_0/V$). All the coefficients in the friction law are determined experimentally for the paper-on-paper system except for the value of η, which is determined as follows. We consider the deflection point at $V = V^*$ from velocity weakening to velocity strengthening; this is determined using $d\mu(D_0/V, V)/dV \mid_{V=V^*} = 0$. This leads to

$$\eta = \frac{b_v}{2V^*}\frac{\exp[\frac{\bar{\mu}}{A}]}{\sqrt{\frac{1}{4}\exp[\frac{2\bar{\mu}}{A}] + 1}}, \tag{26}$$

where $\bar{\mu} = a_v - b_v \ln(V^*/V_0)$. Substituting the experimental values of $a_v = 0.369$, $b_v = 0.014$, $V_0 = 1\mu m/s$, $V^* = 1mm/s$ [2] and $A = 0.011$ [9] into Eq. 26 gives $\eta = 14.0 s/m$.

Using the values given above, the friction coefficient $\mu(D_0/V, V)$ in steady sliding region is shown in Fig. 2, which shows an excellent agreement with experiments [2]. The logarithmic velocity weakening behavior of $\mu(D_0/V, V)$ can be found at low velocities ($\leq 0.1mm/s$); in this regime, the motion of the slider is creep-dominated and the effect of the damping term ηV is negligible. In the high-velocity regime, $\mu(D_0/V, V)$ becomes an increasing function of V which behaves as ηV asymptotically. Hence, the experimentally observed dynamical friction coefficient $\mu_d(V)$ [2] can be described by our simple expression of $\mu(D_0/V, V)$ without imposing any extra condition.

We explore the dynamical phase diagram in control parameter space $(V, K/M)$ by systematically varying V (within 10^{-2} to $10^5 \mu m/s$) and K (within 10^{-1} to $10^5 N/cm$) with $M = 1.2kg$ (this is the value used in the experiment). The phase diagram is shown in Fig. 3. Stick-slip occurs below a bifurcation curve $(K/M)_c(V)$, and steady sliding is found above (or to right of) it. The dots refer to the first steady sliding motions observed when increasing K or V. The phase diagram consists of a creep-dominated regime which can be characterized by the time scale $\tau_{cr} = D_0/V$ at low velocities and an inertial regime with a characteristic time $\tau_{in} = 2\pi(M/K)^{1/2}$ at higher velocities. The dashed line indicates $\tau_{cr} = \tau_{in}$. In the creep-dominated (low-velocity) regime, the bifurcation occurs at a constant K/M ($\approx 1.58 \times 10^3 N/cm \cdot kg$). Fig. 4(a) shows the bifurcation from stick-slip to steady sliding as K is increased in this regime. The bifurcation in the inertial (high-velocity) regime, on the other hand, occurs at a constant V ($\approx 1.28 \times 10^3 \mu m/s$). The bifurcation from stick-slip to steady sliding in this regime is shown in Fig. 4(b). Except for the finite slope of the experimental bifurcation curve which we are not able to reproduced, our theoretical phase diagram agrees reasonably well with the experimental phase diagram.

To investigate the nature of the bifurcation, we have measured the amplitude and period of the stick-slip oscillation by using different K and V. The results are shown in Fig. 5. The amplitude and period decrease as the stiffness K is increased. The amplitude approaches zero continuously as K becomes larger and larger; this suggests that the bifurcation from stick-slip to steady sliding by increasing K is a direct Hopf bifurcation. This agrees with previous theoretical and numerical analysis [2,9]. On the other hand, the transition from stick-slip with a finite amplitude to steady sliding (with zero amplitude) when increasing the pulling velocity V is rather sharp (the transition velocity is around $1.28 \times 10^3 \mu m/s$). This supports that the bifurcation encountered by increasing velocity is of the inverted Hopf type as was suggested previously [1,2,12] based on experimental data (but was not understood theoretically). We have shown numerically that the inverted Hopf bifurcation can be obtained within our fricition model.

V. CONCLUSION

We have shown that the phenomenological description of dry friction proposed by Baumberger et al. is equivalent to the friction law of Rice and Ruina in the case of small deviation from the constant sliding motion. We extend

the phenomenological description of Baumberger et al. and construct a simple model that can be used to simulate dynamics of dry friction in various regimes. We have shown that, by associating the thermally activated creeping motion with a damping term which is significant only when the velocity is large, the model gives rise to satisfactory agreement with the experimental phase diagram. Except for the finite slope of the bifurcation curve observed in experiments, the essential features of the bifurcation in both creep-dominated and inertial regime can be reproduced using our simple model. We believe that the model will also be very useful for numerical study of earthquake models which are often modeled using block-spring systems.

[1] T. Baumberger, F. Heslot and B. Perrin, Nature **367**, 544 (1994).
[2] F. Heslot, T. Baumberger, B. Perrin, B. Caroli, and C. Caroli, Phys. Rev. E **49**, 4973 (1994).
[3] A. L. Ruina, J. Geophys. Res. B **88**, 10359 (1983).
J. R. Rice and A. L. Ruina, J. Appl. Mech. **50**, 343 (1983).
[4] F. P. Bowden and D. Tabor, *Friction and Lubrication of Solids* (Clarendon Press, Oxford, 1950).
[5] E. Rabinowicz, *Friction and Wear of Materials* (Wiley, New York, 1965).
[6] W. F. Brace and J. D. Byerlee, Science **15**, 990 (1966).
[7] C. H. Scholz, *The Mechanics of Earthquakes and Faulting* (Cambridge University Press, Cambridge, 1990), Chap. 2 and references therein.
[8] J. T. Oden and J. A. C. Martins *Computer methods in Appl. Mech. and Engrg.* **52**, 527 (1985).
[9] T. Baumberger, C. Caroli, B. Perrin, and O. Ronsin, Phys. Rev. E **51**, 4005 (1995).
[10] T. Baumberger and L. Gauthier, J. Phys. I (France) **6**, 1021 (1996).
[11] J. R. Rice, J. Geophys. Res. **98**, B6, 9885 (1993).
[12] *Physics of Sliding Friction*, ed. B. N. J. Persson and E. Tosatti (Kluwer, Dordrecht, 1996).

FIG. 1. Schematic block-spring system. The slider with mass M is driven by a pulling velocity V through a spring with stiffness K. The displacement of the center of mass of the slider with respect to the track is x.

FIG. 2. Friction coefficient μ described by Eq. 23 vs the pulling velocity V when the sliding motion is steady. μ changes from velocity weakening to velocity strengthening at $V = V^*(= 1mm/s)$; this gives $\eta = 14.0s/m$.

FIG. 3. Dynamical phase diagram in $(V, K/M)$ space, obtained by varying K and V with $M = 1.2kg$. It consists of a creep-dominated regime which can be characterized by the time scale τ_{cr} and an inertial regime with a characteristic time τ_{in} (see text). The dashed line indicates $\tau_{cr} = \tau_{in}$. The bifurcation curve which is represented by dots, changes from a horizontal line ($K/M \approx 1.58 \times 10^3 N/cm \cdot kg$) to a vertical line ($V \approx 1.28 \times 10^3 \mu m/s$) at the crossover from creep to inertial motion.

FIG. 4. (a) Time evolution of the spring elongation, when crossing the bifurcation curve in low-velocity regime. $V = 5.0\mu m/s$, $M = 1.2Kg$, and (from upper to lower curve) $K = 10^2, 10^3, 10^4 N/cm$. The lowest curve has been shifted vertically by the amount -1.0×10^{-4} for the sake of clarity. (b) The transition from stick-slip to steady sliding in high-velocity regime. $K = 10^2 N/cm$, $M = 1.2Kg$, and (from upper to lower curve) $V = 10^2, 10^3, 10^4 \mu m/s$. The lowest and the second lowest curves have been shifted vertically by the amoumts -5.0×10^{-4} and -2.0×10^{-4} respectively for the sake of clarity.

FIG. 5. (a) Amplitude of the stick-slip oscillations vs the pulling velocity V at various values of K. The amplitude approaches zero continuously as K increases, whereas the transition from stick-slip to steady sliding as V is increased is rather sharp.(b) Period of the stick-slip oscillations vs the pulling velocity V at various K. The period approaches zero continuously either as K or V increases.

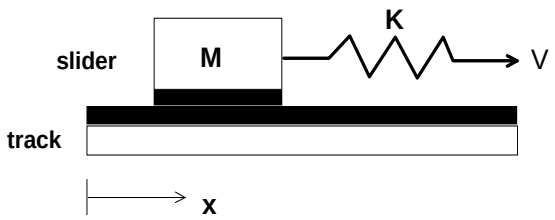

Fig. 1

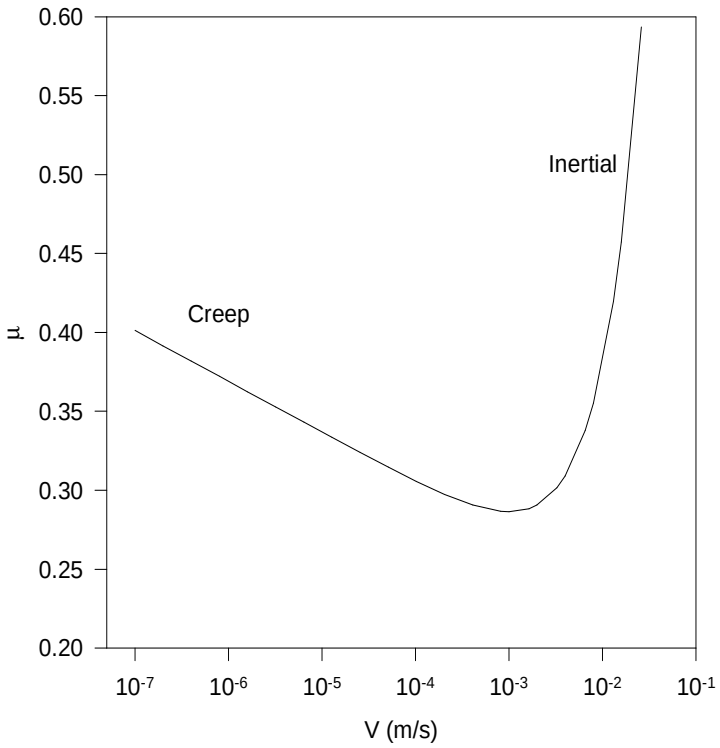
0.60
0.55
0.50
0.45
0.40
0.35
0.30
0.25
0.20
μ
Inertial
Creep
10-7
10-6
10-5
10-4
10-3
10-2
10-1
V (m/s)

Fig. 2

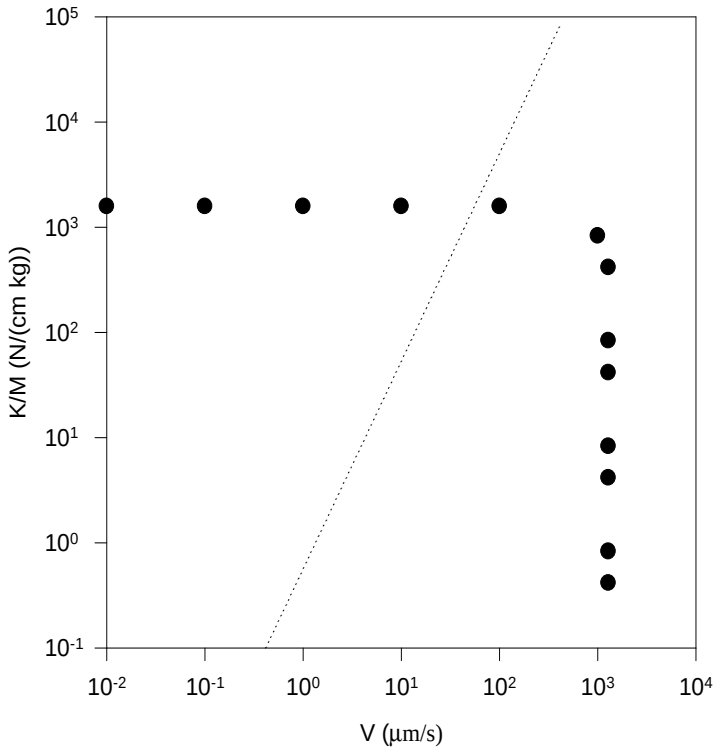
10^5
10^4
10^3
10^2
10^1
10^0
10^-1
K/M (N/(cm kg))
10^-2
10^-1
10^0
10^1
10^2
10^3
10^4
V (μm/s)

Fig. 3

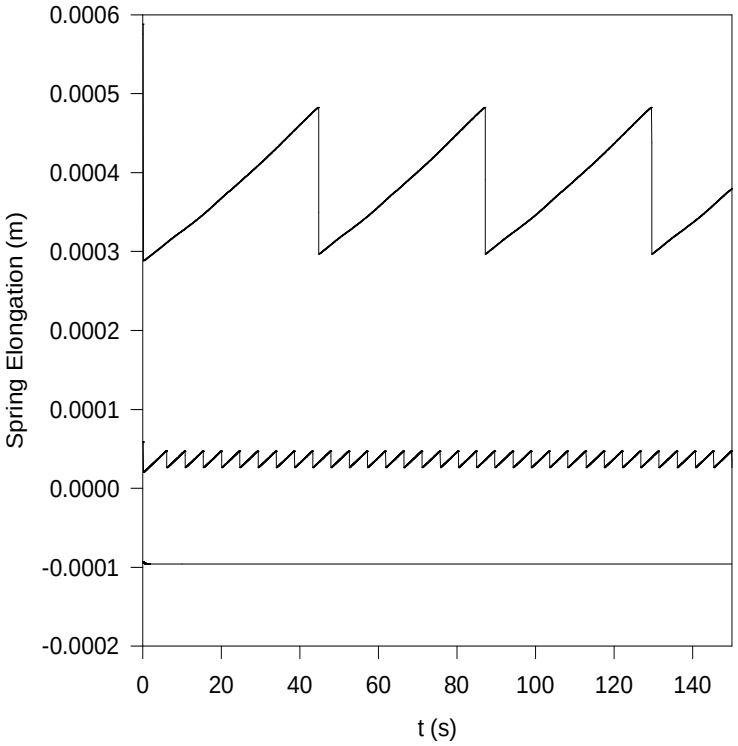
0.0006
0.0005
0.0004
0.0003
0.0002
0.0001
0.0000
-0.0001
-0.0002
Spring Elongation (m)
0
20
40
60
80
100
120
140
t (s)

Fig. 4(a)

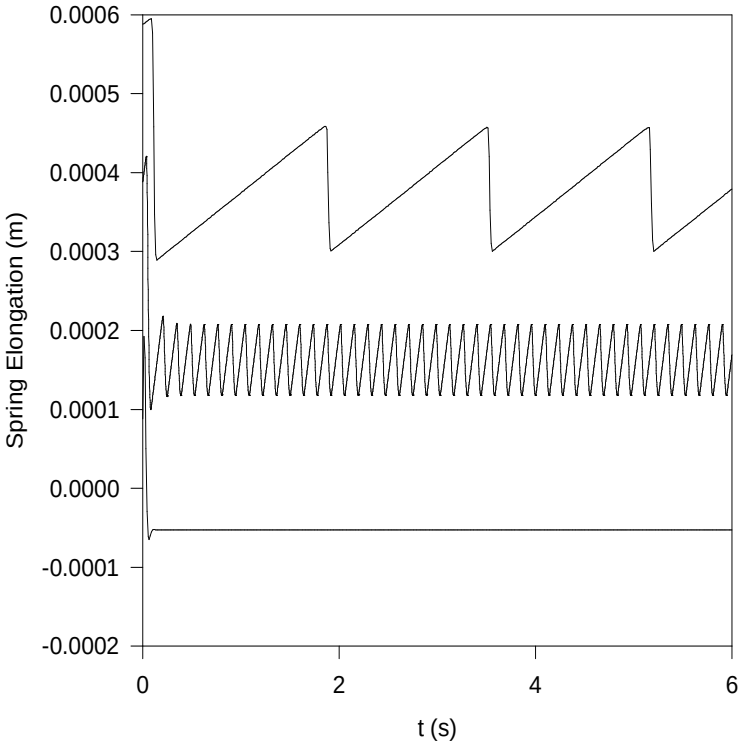
0.0006
0.0005
0.0004
0.0003
0.0002
0.0001
0.0000
-0.0001
-0.0002
Spring Elongation (m)
0
2
4
6
t (s)

Fig. 4(b)

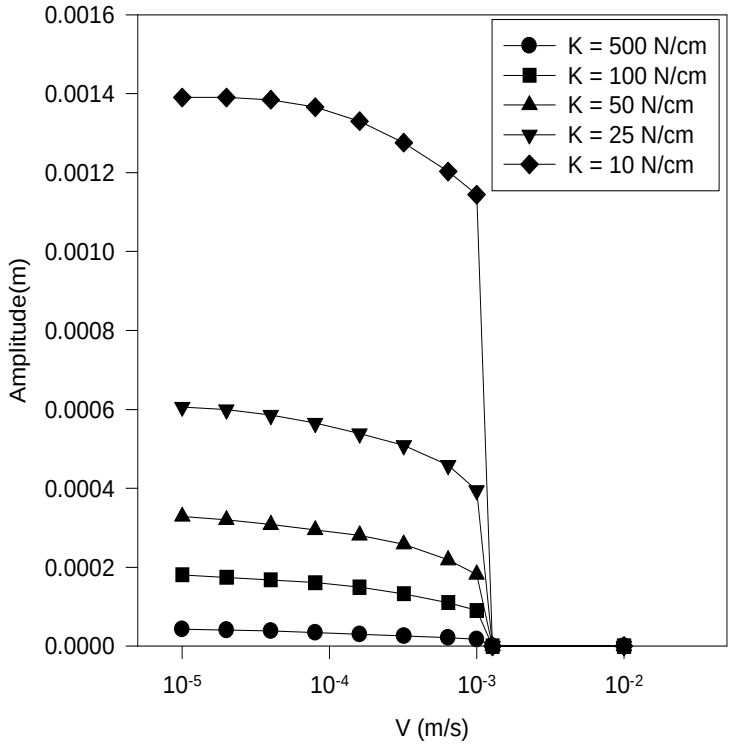
0.0016
0.0014
0.0012
0.0010
0.0008
0.0006
0.0004
0.0002
0.0000
Amplitude(m)
K = 500 N/cm
K = 100 N/cm
K = 50 N/cm
K = 25 N/cm
K = 10 N/cm
10-5
10-4
10-3
10-2
V (m/s)

Fig. 5(a)

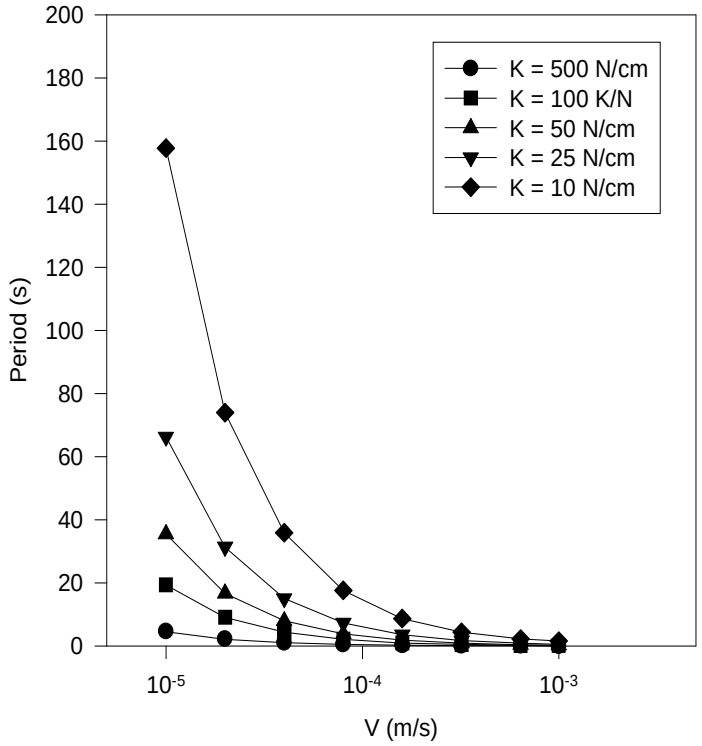
200
180
160
140
120
100
80
60
40
20
0
Period (s)
K = 500 N/cm
K = 100 K/N
K = 50 N/cm
K = 25 N/cm
K = 10 N/cm
10-5
10-4
10-3
V (m/s)

Fig. 5(b)